JOURNAL OF GEOPHYSICAL RESEARCH, VOL. 105, NO. D23, PAGES 28,961–28,977, DECEMBER 16, 2000

Model study of stratospheric chlorine activation and ozone loss during the 1996/1997 winter

M. M. P. van den Broek

Space Research Organization of the Netherlands, Utrecht, Netherlands

A. Bregman and J. Lelieveld

Institute for Marine and Atmospheric Research, Utrecht, Netherlands

Abstract. Chlorine activation and ozone depletion in the Arctic winter stratosphere of 1996–1997 have been studied with a newly developed stratospheric chemistry-transport model (CTM). The chemistry scheme, using a Euler Backward Iterative approximation method, includes a comprehensive set of reactions on ternary aerosol and ice particles, which has been tested against a numerically exact solver. Tracer transports in the CTM are calculated from European Centre for Medium-Range Weather Forecasts (ECMWF) meteorological analyses. Comparisons have been made with O_3 and ClO measurements, and with ozone loss rates derived from observations during February and March 1997. ClO production and ozone depletion are somewhat underestimated by the model. Furthermore, uncertainties regarding the aerosol phase are tested. Assuming nitric acid trihydrate (NAT) particles to form at their melting point, while liquid aerosol is present simultaneously in the model, gives rise to the largest ClO production and the strongest ozone depletion. By correcting for an ECMWF temperature warm bias we obtain a similar large effect on calculated ClO production and ozone depletion for the 1996/1997 Arctic winter, whereas uncertainties in the chlorine abundance seem less important. An average warm bias of 1.3 K at polar stratospheric cloud temperatures on the 50 hPa model level reduces the calculated ozone depletion rates over February and March by 35%. Observations of ClO are reproduced when lower temperatures and maximum Cl_y abundance are assumed, but ozone depletion is slightly overestimated in that case.

1. Introduction

During the last decades, increasing ozone loss has been observed during springtime in the Antarctic lower stratosphere [*Jones and Shanklin*, 1995; *World Meteorological Organization* (*WMO*), 1999]. In the Arctic region, similar chemical ozone loss can occur during cold winters [*Müller et al*., 1997a; *Rex et al*., 1997]. The important contribution of heterogeneous chlorine conversion to these severe ozone losses was recognized shortly after the discovery of the Antarctic ozone hole [*Farman et al*., 1985; *Crutzen and Arnold*, 1986; *Solomon et al*., 1986]. On the surface of polar stratospheric cloud (PSC) particles the chlorine reservoir species HCl and $ClONO_2$ can be converted to HOCl and Cl_2, which are rapidly photodissociated into Cl radicals at sunrise, causing ozone destruction through several catalytic cycles.

Although research efforts on these heterogeneous processes have yielded significant progress, uncertainties remain, for instance, regarding the freezing properties of PSC particles between the ice frost point (~188 K at 50 hPa) and the melting temperature of nitric acid trihydrate (NAT, ~195.5 K at 50 hPa) [*Peter*, 1997]. Observations suggest that both solid and liquid PSC particles are present in this temperature range [*Dye et al*., 1992].

In global gridded chemistry-transport models either NAT formation below its melting temperature is assumed (M. Chipperfield, personal communication, 1999), or the aerosol is assumed to stay liquid down to the ice frost point (F. Lefèvre, personal communication, 1999). In a box model study by *Carslaw et al*. [1997] it is shown that stronger ozone depletion is calculated when the aerosol is assumed to remain liquid until the temperature drops below the ice frost point, as compared to the assumption that only solid particles form. It is yet unclear what the differences are for calculation of chlorine activation and ozone depletion on a large scale, for example, calculated by a three-dimensional (3-D) chemistry-transport model (CTM). Previous 2-D and 3-D model studies [*Portmann et al*., 1996; *Brasseur et al*., 1997] show only a small difference in ozone depletion between these two assumptions in the Antarctic spring. In the Arctic winter, however, temperatures are usually higher, and chlorine is not completely activated throughout the winter. Therefore the phase of the aerosol might be more important in the activation of chlorine and ozone depletion. Besides the uncertainties in aerosol phase, uncertainties regarding the reaction probabilities, temperature, total chlorine, water vapor, HNO_3 concentrations, and aerosol abundance are known to influence the rate of heterogeneous conversion [*Bregman et al*., 1997]. The question arises how important these uncertainties are in the global assessment of chlorine activation and ozone depletion with models.

We present a new stratospheric chemistry model that describes heterogeneous chlorine and bromine reactions on NAT, ice, and liquid particles. The results of the chemistry scheme have been evaluated by comparing the results with those obtained with a numerically exact solver [*Müller et al*.,

Paper number 2000JD900294.
0148-0227/00/2000JD900294$09.00

1994]. The effects of uncertainties in the state of the aerosol on important trace species such as ClO and O_3 have been investigated for different temperatures and assumptions regarding the aerosol phase in the temperature regime between the ice frost point and the NAT melting point. In all cases either NAT, supercooled liquid aerosol, or a combination of the two was assumed.

The newly developed chemistry scheme has been implemented in the 3-D global transport model TM3. Ozone, ClO production, and ozone depletion, as calculated by the model, have been analyzed and compared to observations for the 1996–1997 Arctic winter stratosphere. The uncertainties influencing heterogeneous chemistry have been investigated by performing sensitivity calculations to assess whether these may explain discrepancies between the model results and measurements. The results are discussed in the light of other model uncertainties determining heterogeneous chemistry, such as temperature and chlorine abundance.

2. Description of the TM3 Stratosphere Model

A global three-dimensional CTM, version 3 (TM3), is used, being an extension to the stratosphere of the model described previously by *Houweling et al*. [1998]. The spatial resolution is 5° in longitude by 3.75° in latitude, with 19 vertical layers extending from ground level up to 10 hPa. Near the surface these levels are defined as terrain following sigma coordinates, whereas the stratospheric layers are defined at pressure surfaces. A hybrid of the two is used between the lower levels and the stratosphere.

Six-hourly mean fields of temperature, surface pressure, wind, and humidity from the European Centre for Medium-Range Weather Forecasts (ECMWF) analyses are used to drive the transport of trace species. The reanalyzed ECMWF data have been preprocessed by the Royal Dutch Meteorological Institute (KNMI) to fit the TM3 grid and maintain mass conservation. Every 3 hours the change in concentration through transport is calculated for 25 species and families of species. A second moment advection scheme [*Prather*, 1986] is used to calculate advective transport. For meridional and vertical transport a time step of 45 min is applied, whereas the calculation of zonal transport uses an 18 min time step, which is further reduced near the poles. Convection is calculated with the *Tiedtke* [1989] mass flux parameterization for cumulus clouds, including entrainment and detrainment in updrafts and downdrafts. Tracer transport in TM3 has been tested by comparing radon 222 observations at different locations to model simulations (F. J. Dentener et al., Simulation of the transport of radon 222 using on-line and off-line global models at different horizontal resolutions: A detailed comparison with measurements, submitted to *Journal of Geophysical Research*, 2000). High correlations of model results and measurements were obtained, ranging from $r = 0.5$–0.8. Both anthropogenic (aircraft, industry) and biogenic (lightning, soil) sources of NO_x are included, as well as anthropogenic CO emissions at the surface. A detailed overview of these emissions is given by *Houweling et al*. [1998]. Methane, CFC-11, CFC-12, and N_2O are constrained at ground level according to the values listed in the 1994 Scientific Assessment of Ozone Depletion [*WMO*, 1995]. Dry deposition of reaction products at the surface is calculated using a resistance analogy-based parameterization [*Ganzeveld et al*., 1998]. Wet deposition of soluble trace species is calculated from precipitation rates and Henry's law coefficients [*Houweling et al*., 1998].

At the top level, boundary conditions are maintained for the long-lived trace gases methane, N_2O, CFC-11, and CFC-12, using monthly averaged data of 1992 from the Cryogenic Limb Array Etalon Spectrometer (CLAES) instrument on the UARS satellite [*Roche et al*., 1996; *Nightingale et al*., 1996], and O_3, using climatological data [*Fortuin and Kelder*, 1998]. Total inorganic bromine, chlorine, and odd nitrogen are prescribed in the top three model layers, using observed correlations with N_2O (Br_y [*Daniel et al*., 1996], Cl_y [*Woodbridge et al*., 1995], and NO_y [*Keim et al*., 1997]). The stratospheric growth rates of these species are based on measurements presented by *WMO* [1999]. The model concentrations are adjusted toward the measurements with a relaxation time of 3 days. H_2O in the stratosphere is prescribed by seasonally and zonally averaged data of the Halogen Occultation Experiment (HALOE) over the 5 year period from 1991 to 1996. These data have been validated by *Harries et al*. [1996].

The chemistry routine contains 46 species and 167 reactions relevant to the stratosphere and troposphere. The reaction scheme is listed in Table 1. Thirty heterogeneous chlorine and bromine reactions are included, of which 11 are on ice and on NAT, and 8 are on liquid particles. A Euler Backward Iterative (EBI) scheme is used to solve the photochemical differential equations [*Hertel et al*., 1993].

The reaction scheme is based on a photochemical box model [*Müller et al*., 1994]. Reaction constants of gas phase binary and ternary reactions are taken from *DeMore et al*. [1997]. Photolysis rates are calculated from an updated radiation code, originally developed by *Lary and Pyle* [1991]. Calculations of the absorption cross sections have been updated according to *DeMore et al*. [1997] and extended with additional species (G. Becker, personal communication, 1998). The oxygen and nitric oxide absorption cross sections in the Schumann Runge wavelength band are calculated using the parameterization of *Allen and Frederick* [1982]. The temperature-dependent cross sections are calculated at each chemistry time step. A matrix that lists precalculated values of incoming actinic fluxes, depending on zenith angle, pressure, and latitude, is used to update the diurnal cycle of photolysis rates every 5 days. Every month a new table of actinic fluxes is calculated, using latitudinally varying ozone profiles from the ozone climatology of *Fortuin and Kelder* [1998].

Heterogeneous reaction rates are calculated at each chemistry time step. Zonal mean H_2SO_4 concentrations are taken each month from the results of a two-dimensional microphysical model [*Bekki and Pyle*, 1994]. Effective radius, aerosol surface, and volume are calculated in the model. A lognormal size distribution with a σ value of 1.8, and a constant total aerosol number density of 10 particles cm^{-3}, are assumed throughout the stratosphere. The input H_2SO_4 concentrations have been scaled to impose agreement of the modeled aerosol surface density with observations by the Stratospheric Aerosol and Gas Experiment (SAGE). [*Thomason et al*., 1997]. The physical state of the particles is determined at each time step by comparing the equilibrium vapor pressures of ice and NAT to the H_2O and HNO_3 partial pressures, respectively, using the formulation of *Hanson and Mauersberger* [1988]. In the standard configuration, ice forms 3 K below its equilibrium vapor pressure, with a number density of 0.01 particles cm^{-3}. NAT formation yields a number density of 1 particle cm^{-3} at a supersaturation of 10. This latter assumption implies that an

Table 1. Overview of Reactions and Reaction Rate Constants

Reaction	k_0^{300}	n	k_∞^{300}	m	A	B
Binary Gas Phase Reactions[a]						
$O + O_3 \rightarrow 2\ O_2$					8.e−12[b]	2,060
$O(^1D) + H_2 \rightarrow OH + HO_2$					1.1e−10	0
$O(^1D) + H_2O \rightarrow 2\ OH$					2.2e−10	0
$O(^1D) + N_2O \rightarrow 2\ NO$					6.7e−11	0
$O(^1D) + N_2O \rightarrow N_2 + O_2$					4.9e−10	0
$O(^1D) + CH_4 \rightarrow OH + CH_3O_2$					1.5e−10	0
$3\ O(^1D) + CHCl_3 \rightarrow 3\ Cl$					2.3e−10	0
$2\ O(^1D) + CH_2Cl_2 \rightarrow 2\ Cl$					1.4e−10	0
$O + OH \rightarrow HO_2$					2.2e−11	−120
$O + HO_2 \rightarrow OH + O_2$					3.e−11	−200
$O + H_2O_2 \rightarrow OH + HO_2$					1.4e−12	2,000
$H + O_3 \rightarrow OH + O_2$					1.4e−10	470
$H + HO_2 \rightarrow OH + OH$					8.1e−11 × 0.9	0
$H + HO_2 \rightarrow H_2 + O_2$					8.1e−11 × 0.08	0
$H + HO_2 \rightarrow O + H_2O$					8.1e−11 × 0.02	0
$OH + O_3 \rightarrow HO_2 + O_2$					1.6e−12	940
$OH + H_2 \rightarrow H_2O + H$					5.5e−12	2,000
$OH + OH \rightarrow O + H_2O$					4.2e−12	240
$OH + HO_2 \rightarrow H_2O + O_2$					4.8e−11	−250
$OH + H_2O_2 \rightarrow H_2O + HO_2$					2.9e−12	160
$HO_2 + O_3 \rightarrow OH + O_2$					1.1e−14	500
$HO_2 + HO_2 \rightarrow H_2O_2 + O_2$					2.3e−13	−600
$O + NO_2 \rightarrow NO + O_2$					6.5e−12	−120
$O + NO_3 \rightarrow NO_2 + O_2$					1.e−11	0
$H + NO_2 \rightarrow NO + OH$					4.e−10	340
$OH + NO_3 \rightarrow NO_2 + HO_2$					2.2e−11	0
$OH + HNO_2 \rightarrow NO_2 + H_2O$					1.8e−11	390
$OH + HNO_4 \rightarrow NO_2 + H_2O + O_2$					1.3e−12	−380
$OH + HNO_3 \rightarrow H_2O + HNO_3$					see note[c]	
$HO_2 + NO \rightarrow NO_2 + OH$					3.5e−12	−250
$HO_2 + NO_3 \rightarrow OH + NO_2 + O_2$					1.2e−11	0
$N + O2 \rightarrow NO + O$					1.5e−11	3,600
$N + NO \rightarrow N2 + O$					2.1e−11	−100
$NO + O_3 \rightarrow NO_2 + O_2$					2.e−12	1,400
$NO_3 + NO \rightarrow 2\ NO_2$					1.5e−11	−170
$NO_2 + O_3 \rightarrow NO_3 + O_2$					1.2e−13	2,450
$OH + CO \rightarrow HO_2 + CO_2$					1.5e−13 × $(1 + 0.6P_{atm})$	
$OH + CH_4 \rightarrow H_2O + CH_3O_2$					2.45e−12	1,775
$OH + CH_2O \rightarrow HO_2 + CO + H_2O$					1.e−11	0
$OH + CH_3OH \rightarrow HO_2 + CH_2O + H_2O$					6.7e−12	600
$OH + CH_3O_2H \rightarrow CH_3O_2 + H_2O$					3.8e−12 × 0.7	−200
$OH + CH_3O_2H \rightarrow CH_2O + H_2O + OH$					3.8e−12 × 0.3	0
$HO_2 + CH_3O_2 \rightarrow CH_3O_2H + O_2$					3.8e−13	−800
$CH_3O_2 + CH_3O_2 \rightarrow CH_2O + CH_3OH + O_2$					2.5e−13	−190
$CH_3O_2 + NO \rightarrow CH_2O + NO_2 + HO_2$					3.e−12	−280
$O + ClO \rightarrow Cl + O_2$					3.e−11	−70
$O + OClO \rightarrow ClO + O_2$					2.4e−12	960
$O + HCl \rightarrow Cl + OH$					1.0e−11	3,300
$O + HOCl \rightarrow OH + ClO$					1.7e−13	0
$OH + Cl_2 \rightarrow Cl + HOCl$					1.4e−12	900
$OH + ClO \rightarrow HO_2 + Cl$					1.1e−11 × 0.94	−20
$OH + ClO \rightarrow HCl + O_2$					1.1e−11 × 0.06	−20
$OH + OClO \rightarrow HOCl + O_2$					4.5e−13	−800
$OH + HCl \rightarrow Cl + H_2O$					2.6e−12	350
$OH + HOCl \rightarrow ClO + H_2O$					3.e−12	500
$HO_2 + Cl \rightarrow HCl + O_2$					1.8e−11	−170
$HO_2 + Cl \rightarrow ClO + OH$					4.1e−11	450
$HO_2 + ClO \rightarrow HOCl + O_2$					4.8e−13 × 0.97	−700
$HO_2 + ClO \rightarrow HCl + O_3$					4.8e−13 × 0.03	−700
$NO + OCLO \rightarrow NO_2 + ClO$					2.5e−12	600
$Cl + O_3 \rightarrow ClO + O_2$					2.9e−11	260
$Cl + H_2 \rightarrow HCl + HO_2$					3.7e−11	2,300
$Cl + H_2O_2 \rightarrow HO_2 + HCl$					1.1e−11	980
$Cl + CH_4 \rightarrow HCl + CH_3O_2$					1.1e−11	1,400
$Cl + CH_2O \rightarrow HCl + CO + HO_2$					8.1e−11	30
$Cl + CH_3OH \rightarrow HO_2 + CH_2O + HCl$					5.4e−11	0
$Cl + OClO \rightarrow 2\ ClO$					3.4e−11	−160
$Cl + Cl_2O_2 \rightarrow Cl_2 + O_2 + Cl$					1.e−10	0
$Cl + HOCl \rightarrow Cl2 + OH$					2.5e−12	130
$Cl + ClONO_2 \rightarrow Cl_2 + NO_3$					6.5e−12	−135
$ClO + NO \rightarrow NO_2 + Cl$					6.4e−12	−290

Table 1. (continued)

Reaction	k_0^{300}	n	k_∞^{300}	m	A	B
Binary Gas Phase Reactions[a] (continued)						
$ClO + CH_3O_2 \rightarrow HO_2 + Cl + CH_2O$					3.3e−12	115
$O + BrO \rightarrow Br + O_2$					1.9e−11	−230
$O + HBr \rightarrow OH + Br$					5.8e−12	1,500
$O + HOBr \rightarrow OH + BrO$					1.2e−10	430
$OH + HBr \rightarrow Br + H_2O$					1.1e−11	0
$HO_2 + Br \rightarrow HBr + O_2$					1.5e−11	600
$HO_2 + BrO \rightarrow Br + OH + O_2$					3.4e−12	−540
$Br + O_3 \rightarrow BrO + O_2$					1.7e−11	800
$Br + CH_2O \rightarrow HBr + CO + HO_2$					1.7e−11	800
$Br + OClO \rightarrow BrO + ClO$					2.6e−11	1,300
$BrO + NO \rightarrow NO_2 + Br$					8.8e−12	−260
$BrO + ClO \rightarrow Br + OClO$					1.6e−12	−430
$BrO + ClO \rightarrow Br + Cl + O_2$					2.9e−12	−220
$BrO + ClO \rightarrow BrCl + O_2$					5.8e−13	−170
$BrO + BrO \rightarrow 2\ Br + O_2$					1.5e−12	−230
Ternary Gas Phase Reactions[d]						
$O + O_2 + M \rightarrow O_3 + M$	6.e−34	2.3	···	···	···	···
$H + O_2 + M \rightarrow HO_2 + M$	5.7e−32	1.6	7.5e−11	0	···	···
$OH + OH + M \rightarrow H_2O_2 + M$	6.2e−31	1.	2.6e−11	0	···	···
$O + NO + M \rightarrow NO_2 + M$	9.e−32	1.5	3.e−11	0	···	···
$OH + NO + M \rightarrow HNO_2 + M$	7.e−31	2.6	3.6e−11	0	···	···
$OH + NO_2 + M \rightarrow HNO_3 + M$	2.5e−30	4.4	1.6e−11	1.7	···	···
$HO_2 + NO_2 + M \rightarrow HNO_4 + M$	1.8e−31	3.2	4.7e−12	1.4	2.1e27	10,900
$NO_2 + NO_3 + M \rightarrow N_2O_5 + M$	2.2e−30	3.9	1.5e−12	0.7	2.7e−27	11,000
$CH_3O_2 + NO_2 + M \rightarrow CH_3O_2NO_2 + M$	1.5e−30	4.0	6.5e−12	2.0	1.3e−28	11,200
$Cl + NO_2 + M \rightarrow ClNO_2 + M$	1.3e−30	2.0	1.e−10	1.0	···	···
$ClO + NO_2 + M \rightarrow ClONO_2 + M$	1.8e−30	3.4	1.5e−11	1.9	···	···
$ClO + ClO + M \rightarrow Cl_2O_2 + M$	2.2e−32	3.1	3.5e−12	1.0	1.3e−27	8,744
$BrO + NO_2 + M \rightarrow BrONO_2 + M$	5.2e−31	3.2	6.9e−12	2.9	···	···
Photodissociation Reactions[e]						
O_2[5] $+ h\nu \rightarrow O + O$						
$O_3 + h\nu \rightarrow O_2 + O(^1D)$						
$O_3 + h\nu \rightarrow O_2 + O$						
$HNO_3 + h\nu \rightarrow OH + NO_2$						
$N_2O_5 + h\nu \rightarrow NO_2 + NO_3$						
$ClONO_2 + h\nu \rightarrow Cl + NO_3$						
$NO + h\nu \rightarrow N + O$						
$H_2O_2 + h\nu \rightarrow OH + OH$						
$Cl_2O_2 + h\nu \rightarrow Cl + Cl + O_2$						
$Cl_2 + h\nu \rightarrow Cl + Cl$						
$HOCl + h\nu \rightarrow Cl + OH$						
$ClNO_2 + h\nu \rightarrow Cl + NO_2$						
$NO_2 + h\nu \rightarrow NO + O$						
$HNO_4 + h\nu \rightarrow HO_2 + NO_2$						
$NO_3 + h\nu \rightarrow NO + O_2$						
$NO_3 + h\nu \rightarrow NO_2 + O$						
$CH_2O + h\nu \rightarrow 2\ HO_2 + CO$						
$CH_2O + h\nu \rightarrow H_2 + CO$						
$BrONO_2 + h\nu \rightarrow Br + NO_3$						
$OClO + h\nu \rightarrow O + ClO$						
$BrCl + h\nu \rightarrow Br + Cl$						
$H_2O + h\nu \rightarrow OH + H$						
$HCl + h\nu \rightarrow H + Cl$						
$HOBr + h\nu \rightarrow OH + Br$						
$Br_2 + h\nu \rightarrow Br + Br$						
$N_2O + h\nu \rightarrow N_2 + O$						
$CHCl_3 + h\nu \rightarrow 3\ Cl$						
$CH_2Cl_2 + h\nu \rightarrow 2\ Cl$						
$CH_3CCl_3 + h\nu \rightarrow 3\ Cl$						
$CH_3Cl + h\nu \rightarrow Cl$						
$CH_3O_2H + h\nu \rightarrow OH + HO_2 + CH_2O$						

Reaction	γ on NAT	γ on Ice
Heterogeneous Reactions		
On NAT and ice		
$N_2O_5 + H_2O \rightarrow 2\ HNO_3$	0.0003	0.01
$N_2O_5 + HCl \rightarrow ClNO_2 + HNO_3$	0.003	0.03
$ClONO_2 + HCl \rightarrow Cl_2 + HNO_3$	see text	0.3
$ClONO_2 + H_2O \rightarrow HOCl + HNO_3$	see text	0.3

Table 1. (continued)

Reaction	k_0^{300}	n	k_∞^{300}	m	A	B
			Heterogeneous Reactions (continued)			
On NAT and ice						
$BrONO_2 + H_2O \rightarrow HOBr + HNO_3$	0.001	0.3				
$BrONO_2 + HCl \rightarrow BrCl + HNO_3$	0.3	0.3				
$HCl + HOCl \rightarrow H_2O + Cl_2$	see text	0.3				
$HCl + HOBr \rightarrow BrCl + H_2O$	0.1	0.3				
$HBr + ClONO_2 \rightarrow BrCl + HNO_3$	0.3	0.3				
$HBr + HOCl \rightarrow BrCl + H_2O$	0.3	0.3				
$HBr + HOBr \rightarrow Br_2 + H_2O$	0.1	0.1				
On/in liquid aerosol[f]						
$N_2O_5 + H_2O \rightarrow 2\ HNO_3$						
$ClONO_2 + HCl \rightarrow Cl_2 + HNO_3$						
$ClONO_2 + H_2O \rightarrow HOCl + HNO_3$						
$BrONO_2 + H_2O \rightarrow HOBr + HNO_3$						
$HCl + HOCl \rightarrow H_2O + Cl_2$						
$HCl + HOBr \rightarrow BrCl + H_2O$						
$HBr + HOCl \rightarrow BrCl + H_2O$						
$HBr + HOBr \rightarrow Br_2 + H_2O$						

[a]Reaction rates constants are calculated according to $k(T) = A \exp(-B/T)$.

[b]Read 8.e−12 as 8×10^{-12}.

[c]Here $k = k_1 + (k_3[M]/1 + k_3[M]/k_2)$ with $k_1 = 7.2e{-}15 \times \exp(785/T)$, $k_2 = 4.1e{-}16 \times \exp(1440/T)$, $k_3 = 1.9e{-}33 \exp(7275/T)$, and [M] = the air density (in molecules cm^{-3}).

[d]Reaction rate constants k (molecules $cm^{-3}\ s^{-1}$) are calculated as follows: $k_0(T) = k_0^{300}(T/300)^{-n}$; $k_\infty(T) = k_\infty^{300}(T/300)^{-m}$; $k(T, [M]) = (k_0[M]/1 + k_0[M]/k_\infty) \times 0.6\ 1/1 + \log(k_0[M]/k_\infty)^2$ for temperature T and air density M (in molecules cm^{-3}). The rate constants for the backward reactions are calculated as $A \exp(B/T)$.

[e]Photolysis rates are calculated as follows: $J = \int I(\lambda)\varphi(\lambda, T)\sigma(\lambda, T)\, d\lambda$; $I(\lambda)$ = actinic flux (1/s); $\varphi(\lambda, T)$ = quantum yield, values taken from *DeMore et al.* [1997]; $\sigma(\lambda, T)$ = absorption cross section, values taken from *JPL* [1998], except for absorption cross sections for the Schumann Runge band which are obtained from *Allen and Frederick* [1982].

[f]See text.

undercooling of 3 K is needed for formation of NAT at 50 mbar. Ice, NAT, and supercooled ternary solution droplets are allowed to be present simultaneously. When the temperature is low enough, ice is formed before NAT, which is formed before liquid droplets. The aerosol composition is thus calculated from the remaining gas phase H_2O and HNO_3 concentrations. This order in which PSC particles are formed in the model is rather arbitrary. However, a box model study showed no difference in resulting chlorine distribution and ozone concentrations when the order was reversed, since only small differences in the surface area of NAT and liquid particles occurred.

First-order reaction constants on solid PSCs are taken from *DeMore et al*. [1997] when available. The reaction probabilities of $ClONO_2$ with HCl and H_2O and of HOCl with HCl on NAT are changing with the HCl partial pressure [*Hanson and Ravishankara*, 1995; *Carslaw et al*., 1997]. A correction is made for gas phase diffusion. The abundance, size, and composition of liquid aerosol are calculated from the gas phase H_2O, HNO_3, and H_2SO_4 partial pressures and temperature, using an analytical expression developed by *Carslaw et al*. [1995]. The reaction probabilities of the reactions of $ClONO_2$ with H_2O and HCl, and the reaction of HOCl with HCl in liquid droplets, are calculated with the parameterizations from *Hanson and Ravishankara* [1994] and *Hanson et al*. [1994], respectively. The reaction probability of the $BrONO_2$ hydrolysis is taken from *Hanson et al*. [1996]. Solubilities of HOCl and HOBr are calculated as by *Huthwelker et al*. [1995], assuming a HOBr solubility of 18 times that of HOCl, in line with laboratory results of *Hanson and Ravishankara* [1995]. The parameterization of *Luo et al*. [1995] is used for calculation of the HCl and HBr solubility. Sedimentation of solid particles and subsequent (de)nitrification and (de)hydration have been taken into account by assuming constant fall velocities for NAT and ice particles (M. Chipperfield, personal communication, 1999).

3. Evaluation of the Chemistry Scheme

3.1. Validation of the Numerical Solver

The EBI approximation method [*Hertel et al*., 1993] was applied to solve the set of differential equations in the stratospheric chemistry scheme that has been included in the TM3 chemistry transport model. This scheme was tested against the chemical box model by *Müller et al*. [1994], which uses the solver FACSIMILE [*Curtis and Sweetenham*, 1987]. The latter is based on a Gear method with a variable time step. This solver is known to be very accurate but computationally expensive.

Meteorological input for the box model was provided by an idealized 90-day trajectory for a typical polar stratospheric winter from January to March (F. Lefèvre, personal communication, 1999). The trajectory includes two periods with temperatures below the threshold of polar stratospheric cloud formation (I and II); see Figure 1a. In period I the temperature decreases to 187 K, ~1 K below the ice frost point at 50 hPa, and to 192 K in period II, ~3 K below the NAT point at 50 hPa. NAT formation occurs below 192.5 K, based on a supersaturation of 10, whereas ice particles are formed at equilibrium. The air pressure is 50 hPa throughout the trajectory. Initially, the two numerical solvers are compared, using an identical, detailed scheme for the calculation of heterogeneous reaction rates [*Carslaw et al*., 1995]. For all species, excellent agreement was obtained between the two numerical solvers. The EBI model was used with a time step of 20 min and 10 iterations. Model comparisons for O_3 and noon values of ClO are shown with solid (Gear) and dashed lines (EBI) in Figures

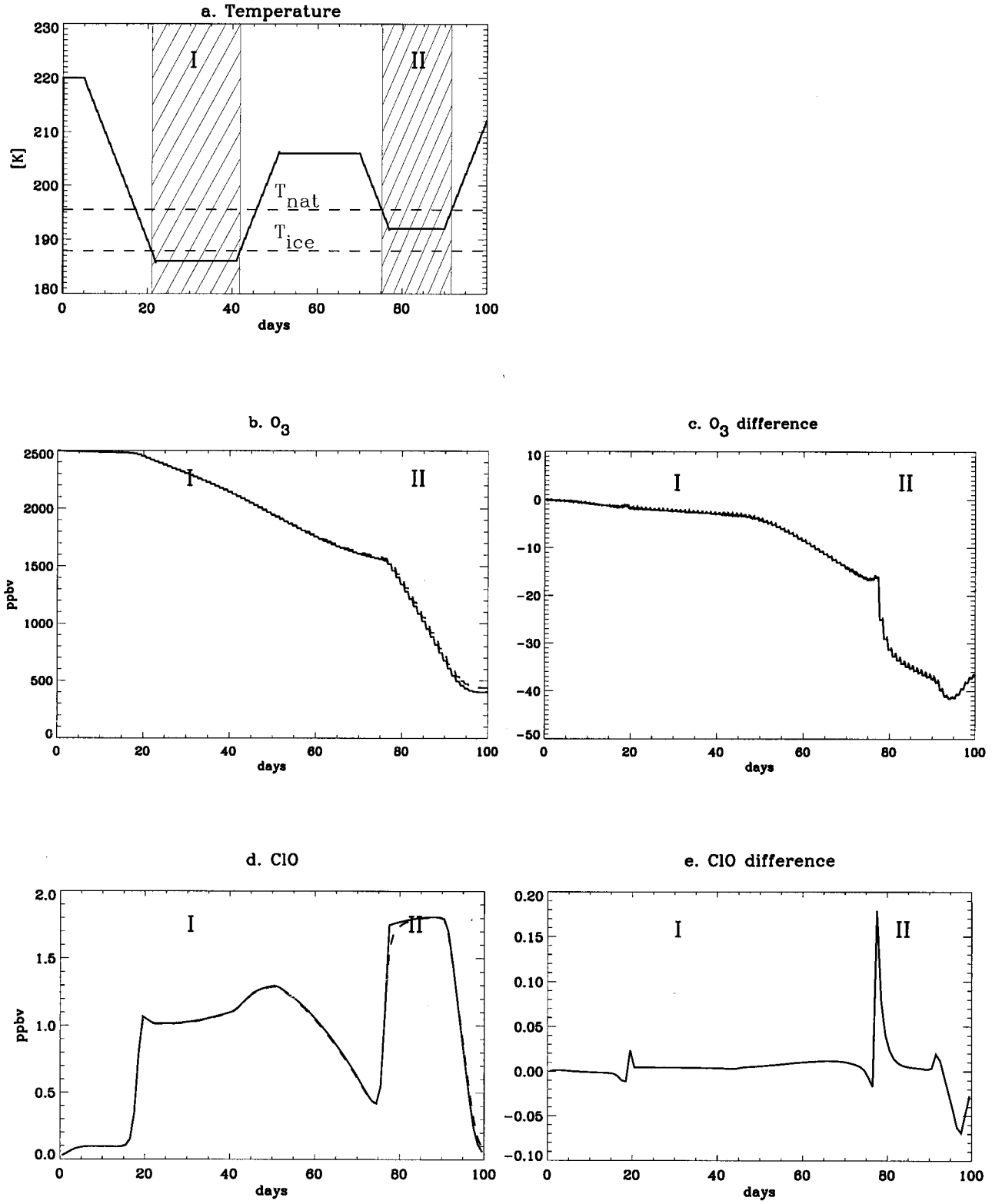

Figure 1. Comparison of the idealized trajectory runs using the EBI chemical scheme and a solver using Gear's method. (a) Temperature along the trajectory with the ice frost temperature T_{ice} and NAT equilibrium temperature T_{nat} indicated by dashed lines and symbols I and II denoting two cold spells with temperatures below T_{ice} and T_{nat}, respectively. (b) and (d) Volume mixing ratios of O_3 and ClO, respectively, at noon (ppbv). Solid lines represent the results of the Gear method; dashed lines denote the EBI results. (c) and (e) Absolute difference in O_3 and ClO (ppbv) between the model using the Gear method and the EBI model.

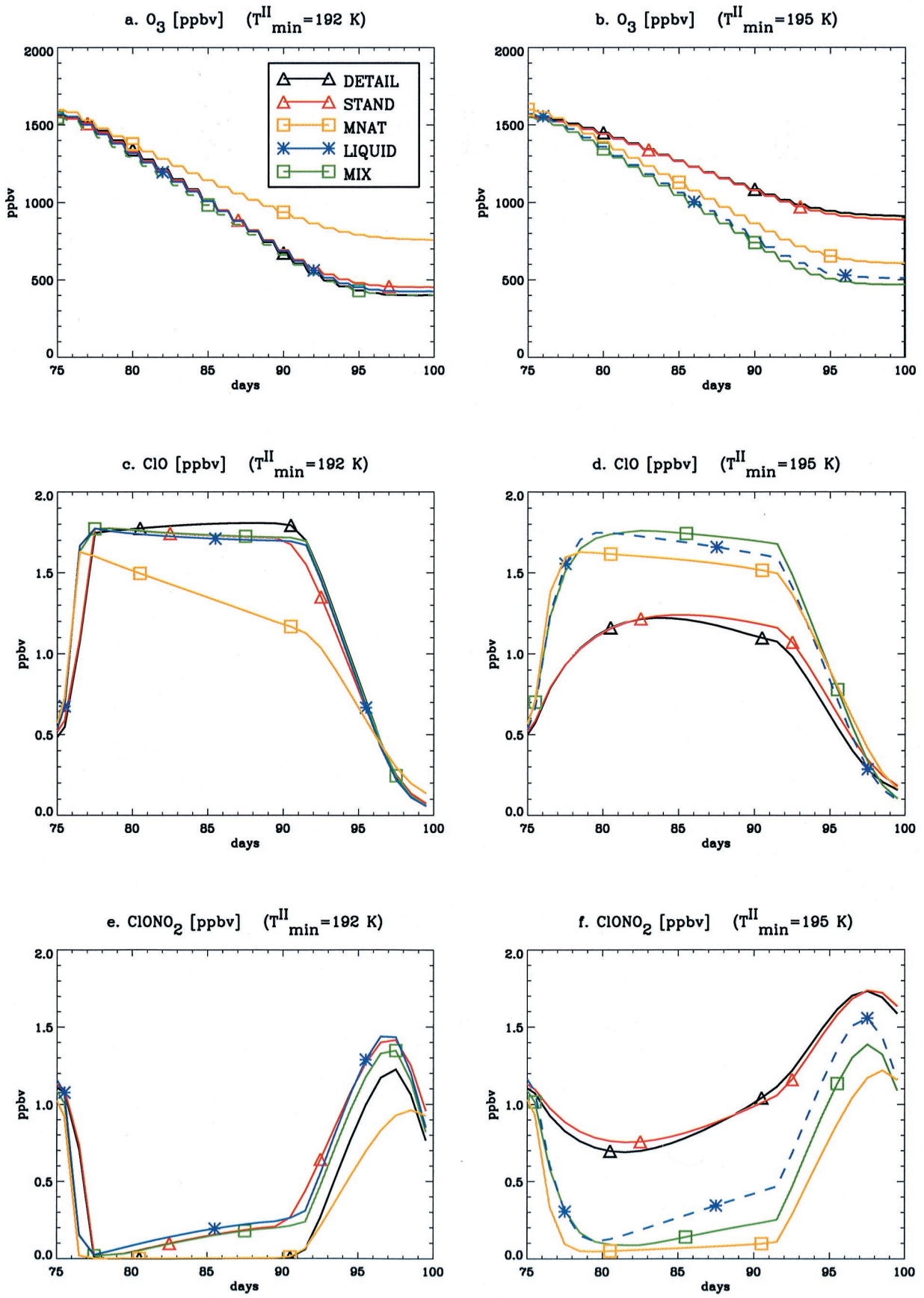

Plate 1. (a) and (b) Calculated O_3 (ppbv), (c) and (d) ClO at noon, and (e) and (f) $ClONO_2$ at noon mixing ratios during period II of the idealized trajectory using the assumptions in Table 2.

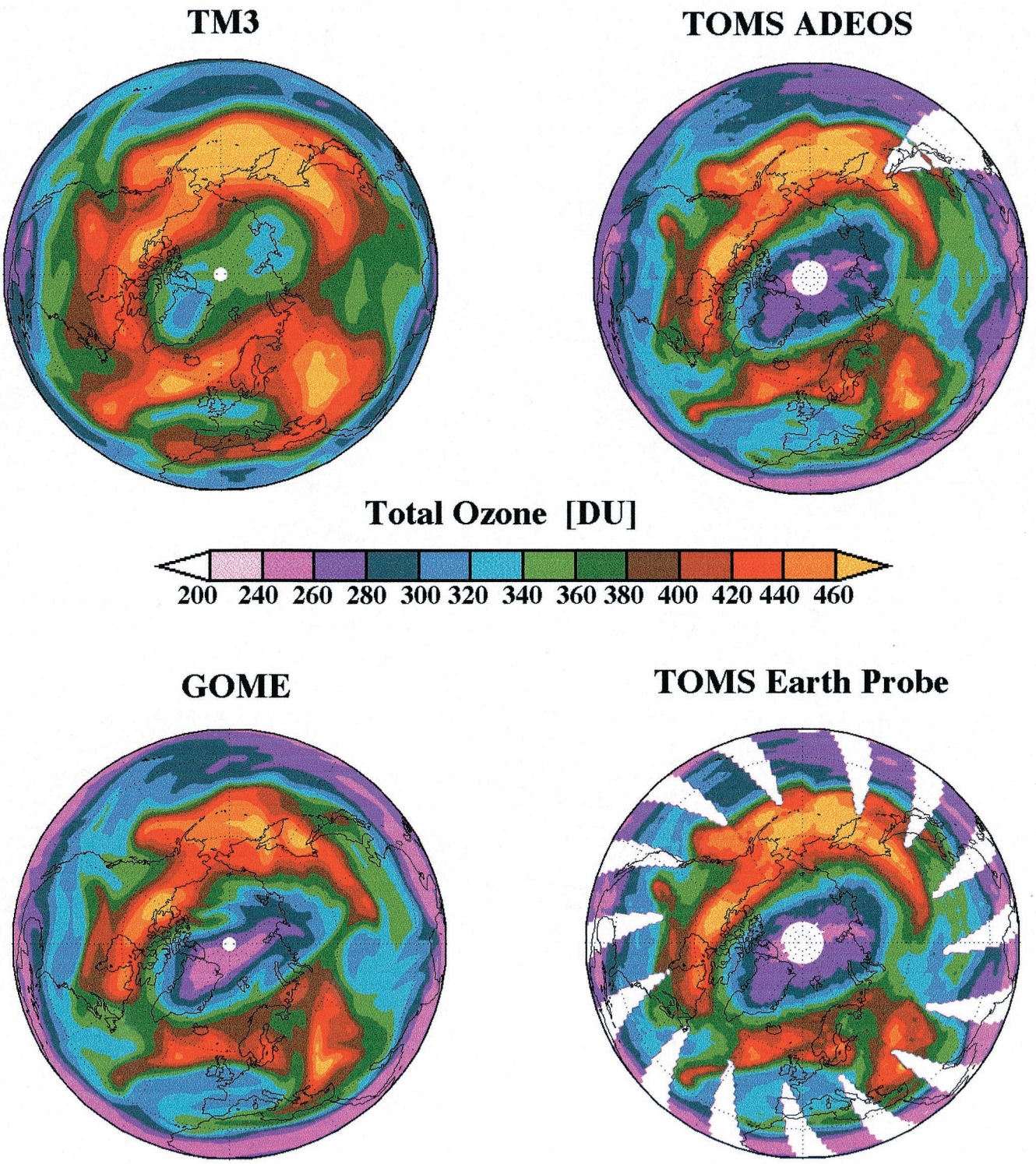

Plate 2. Column ozone measured by three satellite instruments and calculated by the TM3 model on March 27, 1997. (top right) ADEOS TOMS level 3 data. (bottom right) Earth Probe TOMS level 3. (bottom left) GOME level 4. (top left) TM3 results.

1b and 1d. Absolute differences between the two solvers are shown in Figures 1c and 1e for O_3 and ClO, respectively.

3.2. Assumptions in the Aerosol Phase

Calculation of the heterogeneous reaction rates with a global 3-D model requires several simplifying assumptions to limit the computational expense. In the detailed scheme (DETAIL) used in the box model described above, the initial liquid particle number density is 10 particles cm^{-3}, varying with changing temperature and pressure, whereas the aerosol number density is assumed to be constant at 10 particles cm^{-3} in the 3-D model. Also, in TM3 the temperature history of the

Table 2. Model Assumptions, Related to Freezing of PSC Particles Between the Ice Frost Point Minus 3 K and the NAT Equilibrium Temperature[a]

Test Run	Phase History/ Varying Number Density?	Temperature of NAT Formation	NAT, cm^{-3}	Liquid Aerosol, cm^{-3}
DETAIL	yes	at $T < T_{nat} - 3$ K	~1	~9
STAND	no	at $T < T_{nat} - 3$ K	maximum 1	minimum 9
LIQUID	no	none	0	10
MNAT	no	at $T < T_{nat}$	10	0
MIX	no	at $T < T_{nat}$	maximum 1	minimum 9

[a]Model results are depicted in Figure 2.

particles is not considered, and the aerosol phase is only determined by the surrounding temperature and the gas phase concentrations of HNO_3 and H_2O, ignoring the aerosol phase in the previous time step. In other words, it is assumed that NAT forms and evaporates at the same temperature. This might result in an underestimation of the NAT abundance in comparison with the DETAIL scheme since NAT is assumed to form at a supersaturation of 10 (equivalent to 192.5 K at 50 hPa) and only melts at the NAT point, which is 195 K at 50 hPa. This standard configuration (STAND), used in TM3, has been compared to the DETAIL scheme to investigate the effect of these assumptions. In addition to the differences related to the model simplifications, uncertainties exist regarding the phase of the aerosol between the ice frost point and the NAT equilibrium temperature. Several box model runs have been carried out with different assumptions regarding the aerosol phase between the NAT and ice melting temperatures to see what their effect is on chlorine partitioning and ozone depletion. An overview of all test runs and their assumptions is given in Table 2. Both the STAND and DETAIL parameterizations assume that NAT particles form at a supersaturation ratio of 10 of HNO_3 with respect to NAT, which is equivalent to ~3 K undercooling, and the remaining 9 particles are in the liquid phase. Three other assumptions have been tested:

1. In the LIQUID run, no NAT is assumed to form, and the aerosol remains liquid until the ice frost point.

2. The MNAT run assumes that only NAT is present below its melting temperature (10 particles cm^{-3}).

3. The MIX run assumes the formation of 1 particle cm^{-3} of NAT below its melting temperature without the assumption of undercooling, while the other particles remain liquid. Two trajectories have been used for this sensitivity test: the previously described idealized trajectory and a similar trajectory, with higher temperatures during cold period II of the trajectory (195 K instead of 192 K). The results of ClO and $ClONO_2$ (noon values) and O_3, from day 75 onward, are shown in Plate 1. During the first part of the trajectory, when particles are mostly either liquid or water ice, all schemes yield the same results for both the chlorine species and O_3. Whenever water ice forms, chlorine is fully converted into ClO_x (=ClO, Cl_2, and Cl_2O_2) within a day, independent of the assumptions. The lack of sunlight prevents large ozone depletion at this stage. As can be expected, differences appear when temperatures are between the melting points of ice and NAT, as occurs during period II in the trajectories. Note that during cold periods in the Arctic vortex these temperatures are common.

First, we find that the STAND and the DETAIL schemes compare well in both trajectories. Thus the assumptions in TM3, that is, a constant aerosol number density and ignoring the phase history of the particles, do not have a significant influence on the O_3 concentrations and on chlorine activation, especially near the threshold of NAT formation. However, the particle history might have a larger influence on the partitioning of species when the temperature changes occur on smaller timescales.

In the STAND and DETAIL trajectory experiments, NAT is formed at temperatures below 192.5 K, with liquid aerosol present simultaneously. Therefore the resulting species concentrations are similar to the results of the MIX run in the lower temperature trajectory. In the trajectory with higher temperatures during period II, at 195 K, no NAT is formed in the STAND and DETAIL model versions, and they yield the same results as the LIQUID run. Comparing the MNAT and LIQUID results, production of ClO and ozone depletion are stronger when only NAT is formed at temperatures close to the NAT equilibrium temperature, while the LIQUID test case shows stronger ozone depletion in the lower temperature trajectory. At 195 K the NAT surface area is much larger than the area of liquid aerosol, whereas the liquid aerosol volume grows exponentially with decreasing temperatures. At 192 K the liquid particle surface is only about 5 times smaller than that of a NAT particle at the same pressure and gas phase concentrations. This was also found by *Carslaw et al*. [1997]. In addition, the fast reaction of HCl with HOCl in liquid aerosol is a factor of 8 slower on NAT particles at 192 K [*Hanson et al*., 1994; *Hanson and Ravishankara*, 1995]. Remarkably, the MNAT experiments (yellow lines) show that this can even lead to more chlorine activation and ozone loss at 195 K than at 192 K. In the lower temperature trajectory the noon ClO concentrations decrease after initial production because $ClONO_2$ is completely activated through the heterogeneous reactions with HCl and H_2O. Therefore, during the integration, Cl_2 can only be produced from the relatively slow reaction of HCl with HOCl. As a consequence, the ClO production cannot compensate for the gas phase loss of ClO through the HCl production by the CH_4+Cl reaction, and ClO decreases in time. In the higher temperature trajectory, not all $ClONO_2$ is activated at once, so that chlorine activation can continue for a longer time period and more ozone loss is calculated at 195 K than at 192 K when only NAT is present. Although this model situation may not be very realistic, since the influx from neighboring regions would prevent $ClONO_2$ from becoming completely depleted, these results clearly demonstrate the sensitivity and nonlinearity of temperature change on chlorine activation and ozone loss.

In the MIX experiments the largest chlorine activation and ozone depletion is calculated in both trajectories. This is due to the simultaneous presence of NAT and liquid aerosol. The

freezing out of NAT provides a large particle surface area and fast processing of HCl and $ClONO_2$, whereas the reaction of HOCl and HCl in liquid aerosol is able to rapidly convert the remaining reservoir chlorine. It should be noted that a very small difference is found in chlorine activation and ozone loss between the two temperature regimes in the MIX experiment, due to the full conversion of chlorine reservoir species, which occurs already in the higher-temperature trajectory.

The difference in ozone loss between all assumptions regarding the aerosol phase is largest in the trajectory where the minimum temperature in part II is 195 K, close to the NAT melting temperature. Thus the uncertainties regarding the phase of the aerosol have a potentially larger influence on the modeling of ozone loss at temperatures close to the NAT melting temperature.

4. Analysis of Calculated Ozone Fields of February and March 1997

4.1. Total Ozone

The Arctic winter stratosphere in 1996–1997 was characterized by low temperatures below the PSC formation threshold, especially during late winter. *Pawson and Naujokat* [1999] compared this winter to a 32 year record of stratospheric meteorological analyses. Their analysis shows that the vortex region began to cool mid-January, with favorable conditions for PSC formation. It also shows that during March record low temperatures occurred nearly each day of the month at the 30 and 50 hPa pressure levels. The core of this persistent springtime polar vortex, which remained strong and symmetric until late April, was cold enough for formation of type I PSCs until late March [*Coy et al*., 1997]. Consequently, high concentrations of ClO were detected by the Microwave Limb Sounder (MLS) [*Santee et al*., 1997], and strong ozone loss was reported from several measuring and modeling studies [*Manney et al*., 1997; *Müller et al*., 1997b; *Newman et al*., 1997; *Lefèvre et al*., 1998] (see also the November 15, 1997, special issue of *Geophysical Research Letters*.).

In our study the TM3 model, including the STAND chemistry routine, is initialized on October 1, 1996, and integrated until the end of March of the next year. Initialization was based on the results at October 1, 1996, of a multiyear run of the TM3 model, starting in October 1994 [*Bregman et al*., 2000]. The initial ozone concentrations were adjusted by fitting the modeled profiles to Total Ozone Mapping Spectrometer (TOMS) total ozone measurements of October 1, 1996. Model results of total ozone on March 27, 1997, are compared to observations by three satellite instruments in Plate 2. The Global Ozone Monitoring Experiment (GOME) instrument is a nadir-viewing UV-visible light spectrometer (VIS) on board the ERS-2 satellite. For this comparison, assimilated GOME data (level 4) were used [*Eskes et al*., 2000]. The TOMS instruments were flown on board the ADEOS satellite and the NASA Earth Probe (EP) satellite. These instruments are identical and yield similar results, with ADEOS TOMS giving values ~1% higher than EP-TOMS [*Newman et al*., 1997]. The EP-TOMS shows differences with the Dobson network of 1 to 1.5% (R. D. McPeters, personal communication, 2000).

Since the model only extends up to 10 hPa, upper stratospheric ozone has been determined from zonally averaged climatological profiles, based on ozone sonde and satellite measurements between 1980 and 1991 [*Fortuin and Kelder*, 1998], resulting in an additional 30 DU at the poles and 60 DU in the tropics. Overall, the simulated total ozone field and spatial pattern agree well with the observations; however, the model O_3 columns are overestimated up to 60–100 DU within the vortex and up to 20 DU at midlatitudes. Adjusting the model at the top with climatological values of O_3 instead of instantaneous observations has an effect on the total column of ozone as well. Using 5% less ozone, in accord with the Northern Hemisphere annual standard deviations in the climatology [*Fortuin and Kelder*, 1998], resulted in a decrease of 20–30 DU within the vortex and 5–10 DU at midlatitudes.

4.2. Ozone Profiles

Several ozone sonde observations of the same day are compared to the model results in Figure 2. Profiles have been sampled above Aberystwyth (the observation method is described by *Reid et al*. [1996]), Ny Ålesund [*Steinbrecht et al*., 1999], Payerne, Keflavik, Sodankylä, and De Bilt. The model results agree fairly well with the magnitude and height of the ozone peak found in the observations except for Ny Ålesund (Spitsbergen). At this location the model underestimates O_3 above 200 hPa, in line with what is found in the comparison of total ozone (Plate 2). From Plate 2 it can be seen as well that Spitsbergen was located near the vortex edge. A detailed inspection of this plate shows that at this location the TM3 model does not capture the sharp O_3 gradient between the ozone-depleted vortex and the adjacent O_3 maximum, as a consequence of limited model resolution. In general, however, especially between 30 and 73 hPa, the model is in good agreement with all of the observed profiles. An O_3 overestimation is found for the uppermost layer, where climatological mean values are used to constrain the model. In the lowermost stratosphere the model overestimates O_3 in Aberystwyth and De Bilt, both at midlatitudes. At the tropopause (200–300 hPa), ozone is overestimated in comparison with several of the profiles. The latter two effects are probably related to uncertainties in transport processes in the lowermost stratosphere [*Bregman et al*., 2000]. All of these features contribute to the higher O_3 columns as compared to the satellite observations depicted in Plate 2. Furthermore, the vertical fine structure, such as observed over Sodankylä between 70 and 150 hPa, is not captured by the model, due to its relatively coarse vertical resolution.

4.3. Ozone Loss

Next, we discuss the chemical ozone loss during this winter. The top plot of Plate 3 shows the 30 and 40 PV isolines on the 475 K level for March 31, 1997. These lines mark the edge of the vortex, which is defined as the isoline of highest PV gradients on a surface of equal potential temperature. The middle plot shows the chemical ozone depletion at 50 hPa, separately integrated for each grid box over the period of February 1 to March 31, 1997. The maximum chemical ozone depletion is found at the sunlit edge of the vortex region, which is to be expected. These values should be conceived as an upper limit of calculated ozone destruction, if no advection of ozone-depleted air would have taken place. The maximum destruction is 1.3 ppmv, which equals 22 ppbv/d. The ozone-depleted air has been transported throughout the vortex, and this has resulted in decreased ozone concentrations throughout the polar vortex by the end of March. The bottom plot shows the ozone change over this time period as calculated from the full-chemistry run minus the results of a "transport only" run,

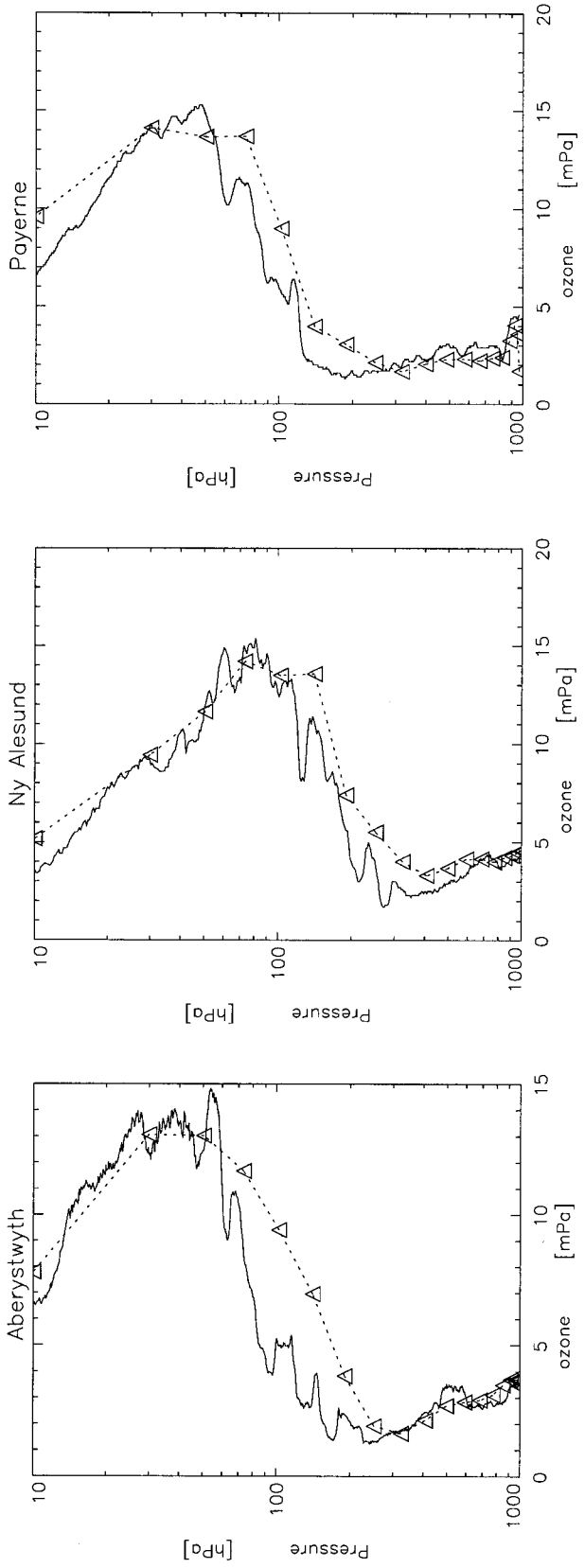

Figure 2. Ozone sonde observations on March 27, 1997 (solid lines), compared to model results of the same day (dashed lines; the triangles denote the center of the model levels). Observations have been carried out at Aberystwyth, Ireland (52.4°N, 4.1°W), Ny Ålesund, Spitsbergen (78.9°N, 12.0°E), Payerne, Switzerland (46.8°N, 7.0°E), Keflavik, Iceland (64.0°N, 22.6°W), Sodankylä, Finland (67.4°N, 26.7°E), and De Bilt, Netherlands (52.1°N, 5.2°E).

in which ozone was treated as a passive tracer. These latter results can be compared to ozone loss rates derived from observations. Inside the vortex, ozone depletion is 0.8 ppmv at most at the 50 hPa level, which is on average 13 ppbv d^{-1}. This is considerably lower than that derived from measurements. *Sinnhuber et al*. [1998] derived ozone loss rates of 22 ppbv d^{-1} at the 475 K level during February and March, derived from ground-based measurements above Ny Ålesund (79.8°N, 11.9°E). Similar values were obtained by *Kreher et al*. [1999] between 475 and 460 K for inner vortex air above Kiruna (67.9°N, 21.1°E). *Schulz et al*. [2000] derived maximum ozone loss rates in the first weeks in March of 45 ppbv d^{-1} during the Match campaign. On average, they inferred a loss of ~20 ppbv d^{-1} during February and March. *Knudsen et al*. [1998] derived an ozone depletion of 1.24 ppmv throughout the vortex at the 475 K level from 154 ozone sonde measurements within the vortex, although their calculations include January as well. All of these measurements accounted for downward transport of O_3 through diabatic cooling. From December to March we calculate a maximum loss of 35 DU in the stratosphere, which is considerably less than the 92 DU derived by *Knudsen et al*. [1998] between January and March and the loss calculated by *Müller et al*. [1997b] in the same period from measurements by HALOE. They calculated loss rates by comparing observed ozone to simultaneous observations of the chemically conserved tracer HF. In general, the model appears to underestimate the ozone loss rates derived from observations.

5. Role of Heterogeneous Chemistry

5.1. ClO Mixing Ratios

Since ozone loss inside the polar vortex is mainly determined by the ClO dimer and BrO-ClO cyles [*Chipperfield and Pyle*, 1998], an underestimation of ozone loss is likely to be caused by underestimated ClO and, to a lesser extent, BrO concentrations. Vertical profiles of ClO have been measured throughout the Northern Hemisphere by MLS on the UARS satellite [*Santee et al*., 1997] during the 1996/1997 winter.

We compare observations of enhanced ClO in the Arctic vortex, sampled on the 46 hPa level of February 20 and February 26, 1997, with model results on 50 hPa. Only daytime ClO measurements were used by *Santee et al*. [1997] to compose a plot for the Northern Hemisphere (Plate 4a). A realistic comparison was obtained by using the local noon model results of these dates. The ClO enhancement, as measured by MLS, is qualitatively reproduced by TM3. On both days, two maxima appear, both in the measurements and in the model, located over Greenland and northern Russia. TM3, however, underestimates the measurements by as much as 1.0 ppbv on different occasions. The single profile precision and accuracy of the MLS level 4 data observations are 0.4 ppbv and 10%, respectively [*Santee et al*., 1997]; however, by averaging several profiles, the precision in the maxima over Greenland and Russia is improved to 0.1–0.2 ppbv. Therefore the difference cannot be explained by possible errors in the observations alone. A similar run, in which the heterogeneous reactions were turned off, illustrated that nearly all ClO calculated by the model in this comparison originates from heterogeneous chemistry. The partitioning of chlorine on February 26 shows that both $ClONO_2$ and HOCl are nearly fully converted at the location of the ClO maxima (together 0.2 ppbv), but 0.6–0.8 ppbv HCl out of 3.3 ppbv Cl_y is still present. The remaining inorganic chlorine is in the form of Cl_2O_2.

The box model study showed that calculated chlorine activation and ozone depletion are strongly influenced by assumptions regarding the phase of the aerosol between the ice frost temperature and the NAT temperature, especially close to the NAT temperature. It was shown that the strongest production of ClO is found when NAT is assumed to form at its melting point, with 1 particle cm^{-3} freezing and the rest of the aerosol remaining in the liquid phase. A sensitivity study was carried out for February 26 using these assumptions on the aerosol phase, resulting in a maximum increase of 0.8 ppbv ClO. The difference with the standard run is shown in Plate 4a. Neither in the atmosphere nor in the laboratory are NAT particles detected ubiquitously between the ice frost point and the NAT point [*Peter*, 1997]. Assuming an overall freezing of NAT below its melting point is likely to give an overestimation of ClO, and the resulting value should therefore be considered as an upper limit regarding the uncertainty of the aerosol phase and its effect on the production of ClO. In addition to these uncertainties related to the aerosol phase, we discuss the previously mentioned model uncertainties affecting heterogeneous reaction rates. *Bregman et al*. [1997] showed with a box model that, within realistic uncertainty ranges, varying the total amount of chlorine and the temperature has the largest impact on ClO. In this study, the values of inorganic chlorine (Cl_y) and temperature have been varied within the uncertainty range to see whether this may explain the discrepancies with the measurements.

For February 25, 1997, *Strunk et al*. [1998] derived the age of air and Cl_y concentrations from organic chlorine species and SF_6 observations within the vortex. Their results are compared to our model results in Figure 3. Polynomial fits have been drawn through both the observations and the model results. The differences between them range from 380–630 parts per trillion by volume (pptv). A sensitivity study has been carried out by adding 500 pptv Cl_y to the model in each grid box. This results in 3.8 ppbv Cl_y at the location of the maximum ClO in Plate 4, which is slightly higher compared to the Cl_y maximum calculated by *Strunk et al*. [1998].

The temperature variability is also known to affect heterogeneous reaction rates. Subgrid-scale temperature variations

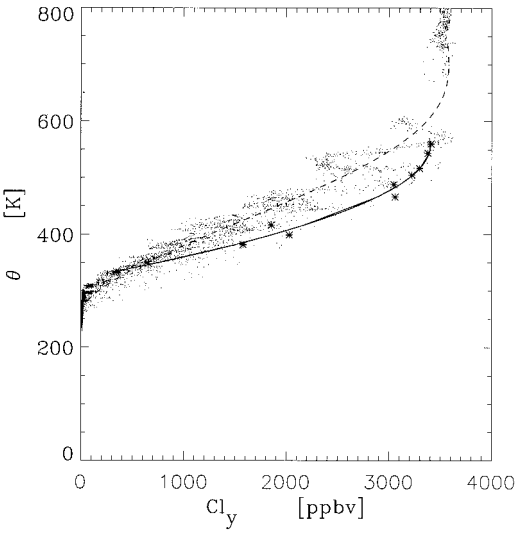

Figure 3. Cl_y within the polar vortex derived from observations (asterisks) and calculated with TM3 (dots) for February 25, 1997. Polynomial fits are indicated by solid and dashed lines, respectively.

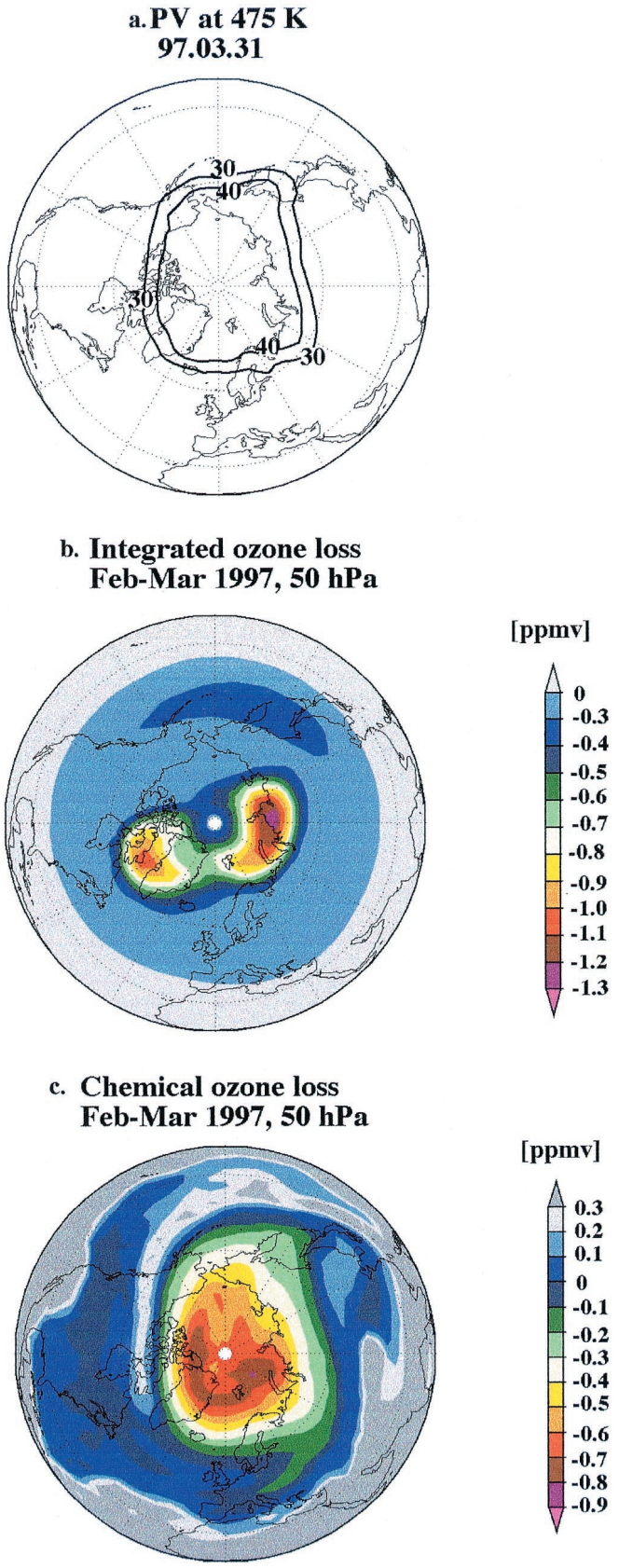

Plate 3. (a) PV values at the 475 K potential temperature level. (b) Chemical ozone destruction integrated for each grid box from February 1 to March 31, 1997, at the 50 hPa model level given in ppmv. (c) Calculated ozone loss in ppmv from February 1 to March 27 as a result of the difference between O_3-O_3 as a passive tracer.

can cause errors in the calculation of heterogeneous chemistry and ozone depletion since the rate of these processes increases nonlinearly with decreasing temperature [*Murphy and Ravishankara*, 1994]. The ECMWF analysis data, used as meteorological input for the TM3 model, indeed show discrepancies with temperature sonde measurements [*Knudsen*, 1996]. Especially at PSC formation temperatures ($T < 195$ K), temperatures are on average overestimated in the ECMWF analyses. The average biases (sonde temperature minus ECMWF temperature) and the standard deviations found by *Knudsen* [1996] at PSC formation temperatures are -0.6 K (± 1.49 K), -1.1 K (± 1.75 K), -1.3 K (± 1.93 K), and -1.6 K (± 2.26 K) at the 100, 70, 50, and 30 hPa levels, respectively.

The differences in ClO with the standard run are shown in Plate 5 for the three test cases: NAT formation below its equilibrium temperature; maximum chlorine abundance; and minimum temperatures. An additional run was carried out in which both the lower temperature limit and the maximum amount of Cl_y are implemented. Both the runs with maximum NAT formation and minimum temperatures significantly enhance the amount of ClO in the model. Any other assumption regarding the freezing of NAT only reduces chlorine activation, as was shown in our box model study. The discrepancies of ECMWF temperatures with temperature sondes, on the other hand, show high variability [*Knudsen*, 1996]. Hence, considering the nonlinear temperature dependency of heterogeneous reaction rates, the temperature uncertainty might well exceed the uncertainty range assumed in this study, and it is probably more important than the aerosol phase uncertainty. A thorough assessment is needed which also takes into account the standard deviation of the temperature biases. A small part of the enhancement in ClO in the top plots of Plate 5 is due to the enhancement of denitrification, which only occurs when NAT is formed. Overall, denitrification was small because temperatures did not decrease below the ice frost point. ClO is enhanced due to the 0.5 ppbv Cl_y increase, as shown in the bottom left plot of Plate 5, but this effect is small compared to the other uncertainties. Since not all chlorine is activated continuously, the surplus Cl_y increases ClO by less than 0.5 ppbv.

By combining the lower temperature and maximum Cl_y abundance in the model, the differences between modeled and observed ClO can be explained, although a small discrepancy remains. Besides the errors in the MLS observations that were mentioned before, subgrid-scale processes which are not captured by the model, such as the additional temperature uncertainty [*Knudsen*, 1996] or lee waves which may cause local temperature decreases of 10 K or more [*Carslaw et al.*, 1998], can possibly explain the remaining differences.

5.2. Ozone Depletion Rates

Maximum ozone depletion was calculated for all sensitivity simulations by substracting the results of the "ozone as a passive tracer" run from those of the full-chemistry runs. The chemical loss that affects the 50 hPa level at the end of March was calculated over February and March 1997. The results are shown in Table 3. Whereas both the temperature decrease and NAT increase have large effects on the calculation of ozone depletion, the large surplus in chlorine only has a small effect because ClO is not fully activated. At lower temperatures, when more chlorine activation takes place, the effect of a chlorine increase is much larger than in the standard run (0.5 ppbv d^{-1} additional ozone depletion instead of 0.3 ppbv d^{-1}). For this winter the uncertainties in aerosol phase and temper-

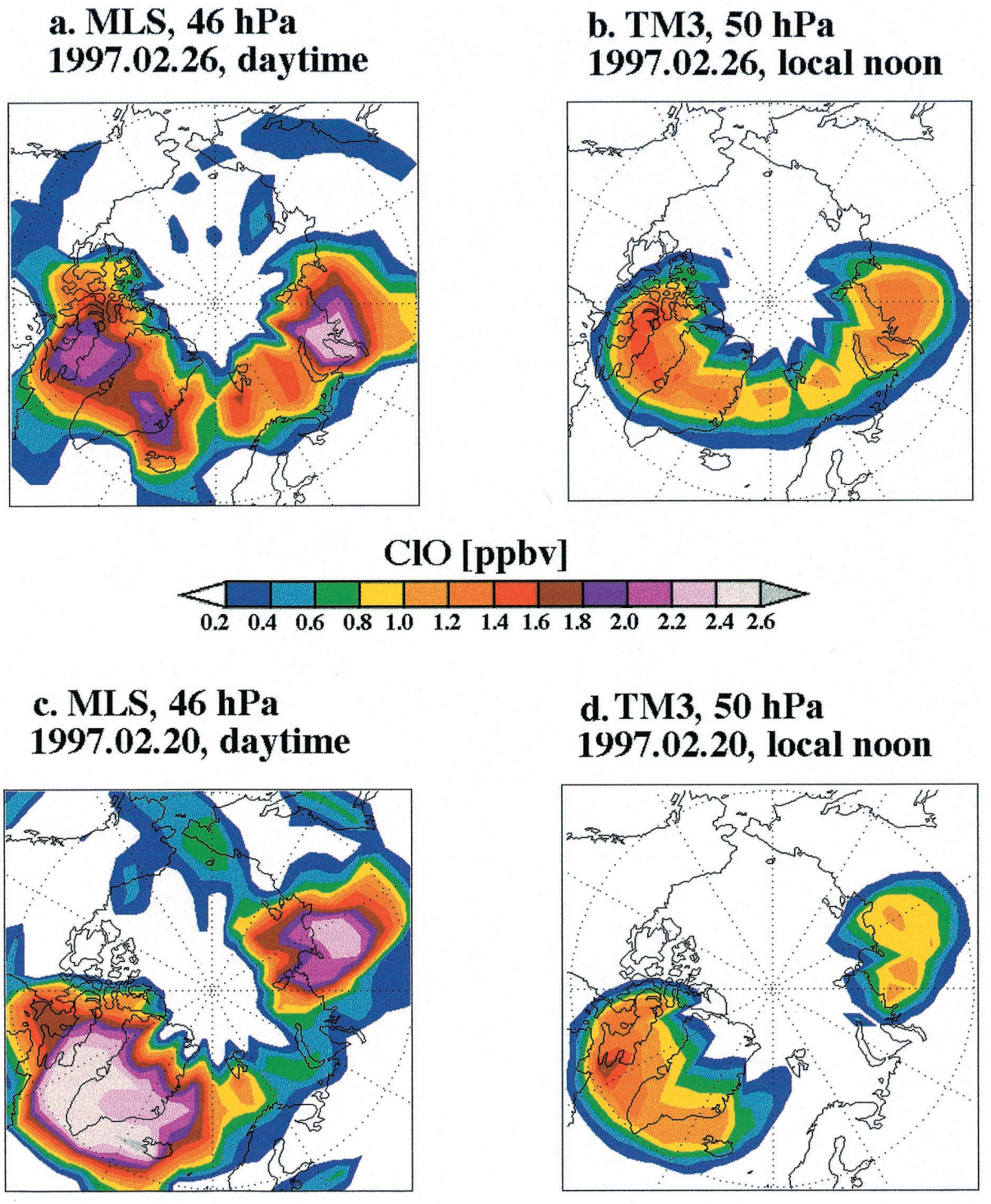

Plate 4. Measured average daytime ClO mixing ratios (ppbv) from MLS at 46 hPa on (a) February 26, 1997, and (c) February 20, 1997. (b) and (d) Modeled ClO mixing ratios (ppbv) at 50 hPa at local noon on the same days.

ature largely determine the uncertainty in calculated chlorine activation and ozone depletion. The model agreement with the measurements improves significantly when temperature is lowered. When maximum Cl_y is assumed as well, ozone depletion is overestimated compared to the observations.

In addition to the discussed uncertainties affecting heterogeneous chemistry, there are uncertainties in the gas phase ClO chemistry. The most important uncertainty influencing ozone depletion is that of the Cl_2O_2 absorption cross section [*Fish and Burton*, 1997]. *Ruhnke et al*. [1999] showed with a 3-D model that the absorption cross section of Cl_2O_2 represents an uncertain factor for the lower stratosphere, and ozone depletion in March 1997 is decreased by 15% at 20 km, when different absorption cross sections are applied. In this study, however, their upper limit absorption cross sections Cl_2O_2 have already been used. Uncertainties in the HCl production

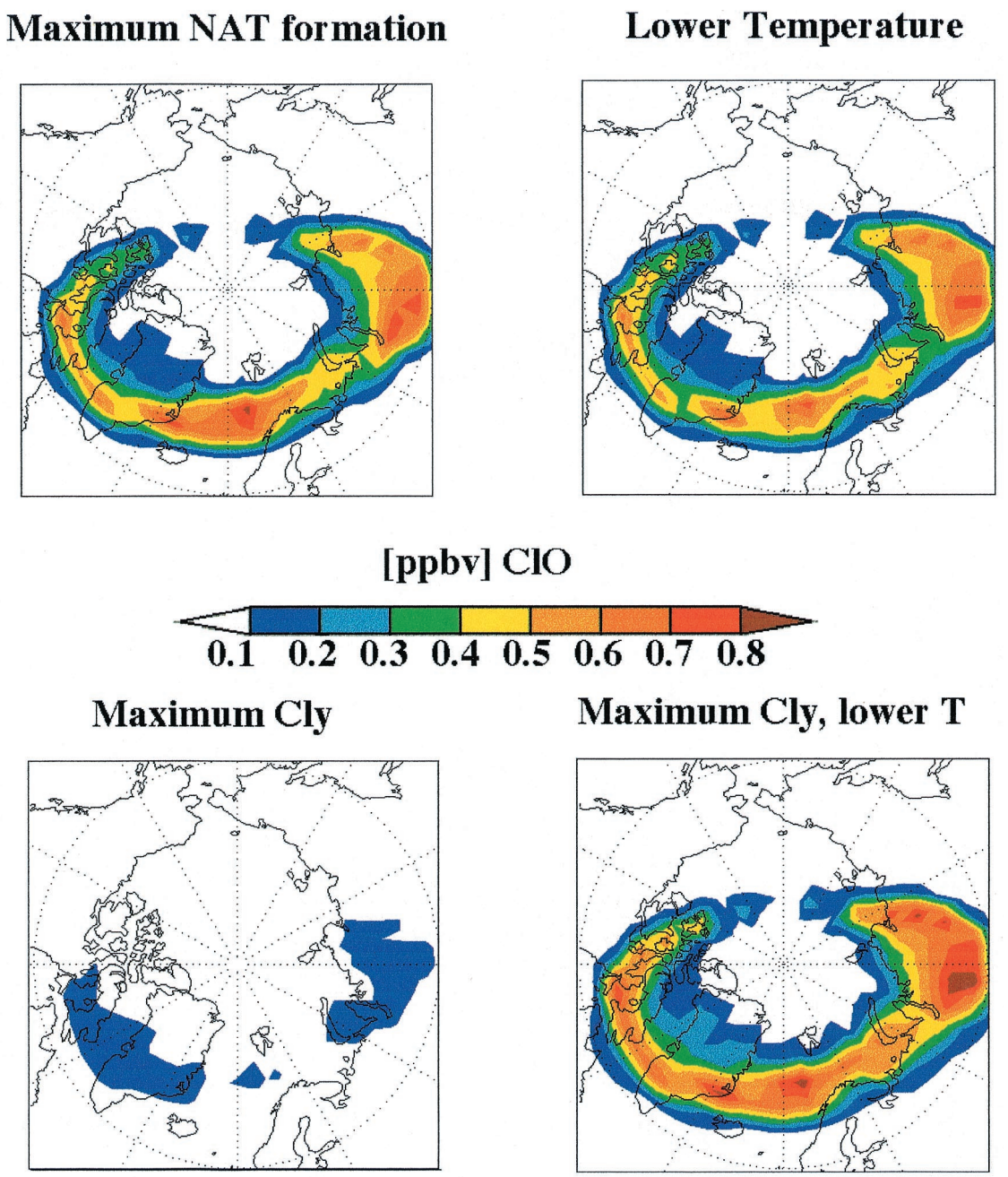

Plate 5. Difference of calculated ClO volume mixing ratios (ppbv) from several test simulations compared with the standard model version at 50 hPa, on February 26, 1997, local noon. (top left) Formation of NAT at its equilibrium temperature. (top right) Temperatures decreased. (bottom left) The 0.5 ppbv increase in inorganic chlorine. (bottom right) Both lower temperatures and increase in Cl_y (see text for details).

Table 3. Sensitivity Simulations With TM3[a]

Test Run	Maximum $-\Delta O_3$ 50 hPa, ppbv d^{-1}, Feb.–March 1997
Standard run	14
NAT formation at equilibrium	21
More Cl_y (6%)	17
Temperature lowered	20
Temperature lowered and increased Cl_y	25

[a]Results indicate maximum modeled ozone depletion during the months of February and March 1997 on the 50 hPa level.

channel from the ClO + HO_2 and ClO + OH reactions have only a small influence in the lower stratosphere [*Ruhnke et al.*, 1999] and are not discussed here.

6. Discussion and Conclusions

We have developed a computationally fast chemistry scheme using a parameterization of heterogeneous chemistry suitable for a 3-D CTM. The results are in excellent agreement with those of a numerically very accurate chemical scheme.

A box model study compares various parameterizations of

NAT formation between the ice frost point and the NAT equilibrium temperature. It shows that maximum chlorine activation and ozone depletion, both at 192 K and at 195 K, is calculated when NAT is assumed to form at its equilibrium temperature, and when liquid particles exist at the same time. Ubiquitous presence of NAT between the ice frost point and the NAT equilibrium temperature is unlikely, and assuming the formation of NAT throughout the stratosphere right below its equilibrium temperature, with liquid aerosol present simultaneously, is not realistic. The resulting calculated chlorine activation should be considered as an upper limit of the surplus ClO that can be modeled by making assumptions on the aerosol phase.

Implementation of the chemistry scheme in a 3-D transport model yields quite good agreement with ozone observations, but production of ClO and ozone depletion are underestimated using the model standard configuration. Adjustment of the microphysical scheme, so that it produces the highest chlorine activation, significantly increases ClO. However, lowering the temperature by only ~1 K at PSC formation temperatures results in a similar increase. Considering that the difference between ECMWF-analyzed temperatures and sonde measurements has not only negative biases but also a large variability, the temperature uncertainty might be even more important than shown here, whereas the microphysical effect is most likely overestimated. The temperature uncertainty therefore appears to be the main problem to realistically model ozone depletion with a 3-D model, and it will therefore be difficult to study the impact of uncertainties in aerosol phase with a 3-D model. Not only the ECMWF temperatures, but also the U.K. Meteorological Office (UKMO) temperatures often used in models, show a warm bias at PSC temperatures [*Knudsen*, 1996]. Therefore underestimation of ClO production and subsequent ozone depletion by models using these temperatures is likely. A more accurate uncertainty estimate cannot be derived from our results, and an assessment accounting for the variability of temperature biases would be useful. When both the temperature biases and the upper uncertainty limit of Cl_y are implemented, the discrepancies with ClO observations remain within the uncertainty ranges of the observations, although ozone depletion is overestimated compared to observations.

In winters with different temperature regimes, the results of such a sensitivity study may be different. Under extremely cold circumstances, such as in the Antarctic springtime stratosphere, full chlorine activation is likely to occur, and both the microphysical and temperature uncertainties (of ~1 K) might have a smaller effect on ozone loss, whereas uncertainties in chlorine abundance are probably more important in such a case. During a winter with higher temperatures, above or close to the NAT equilibrium temperature, the assumption of more NAT formation in the model may affect the calculations of chlorine activation and ozone loss more strongly. Our box model study shows a large difference in O_3 depletion at 195 K, using different parameterizations of NAT formation. Therefore the effects on large-scale calculations under different winter temperature regimes need further investigation.

Acknowledgments. The authors thank A. Piters at KNMI and the Langley-DAAC center for providing total ozone from the GOME and TOMS instruments, respectively, and M. Santee for providing MLS data. P. von der Gathen, E. Kyro, M. Gil, R. Stübi, M. Allaart, and G. Vaughan are acknowledged for providing ozone profile observations through the NILU database, and M. Strunk kindly provided us with values of Cl_y. We thank M. Chipperfield for his denitrification routine and B. Knudsen for calculations of radiosonde-ECMWF temperature biases. Miranda van den Broek was supported by the NWO GO-2 program under project eo-022. Bram Bregman was supported by the European Union (DG-XII) under contracts ENV4-CT95-0155 and ENV4 CT97 0542.

References

Allen, M., and J. E. Frederick, Effective photodissociation cross sections from molecular oxygen and nitric oxide in the Schumann-Runge bands, *J. Atmos. Sci*., *39*, 2066–2074, 1982.

Bekki, S., and J. A. Pyle, A two-dimensional modeling study of the volcanic eruption of Mount Pinatubo, *J. Geophys. Res*., *99*, 18,861–18,869, 1994.

Brasseur, G. P., X. Tie, P. J. Rasch, and F. Lefèvre, A three-dimensional simulation of the Antarctic ozone hole: Impact of anthropogenic chlorine on the lower stratosphere and upper troposphere, *J. Geophys. Res*., *102*, 8909–8930, 1997.

Bregman, A., M. M. P. van den Broek, K. S. Carslaw, R. Müller, T. Peter, M. P. Scheele, and J. Lelieveld, Ozone depletion in the late winter lower Arctic stratosphere: Observations and model results, *J. Geophys. Res*., *102*, 10,815–10,828, 1997.

Bregman, A., J. Lelieveld, M. M. P. van den Broek, P. C. Siegmund, H. Fischer, and O. Bujok, The N_2O and O_3 relationship in the lowermost stratosphere: A diagnostic for mixing processes as represented by a three-dimensional chemistry-transport model, *J. Geophys. Res*., *105*, 17,279–17,290, 2000.

Carslaw, K. S., B. P. Luo, and T. Peter, An analytic expression for the composition of aqueous HNO_3-H_2SO_4 stratospheric aerosol including gas phase removal of HNO_3, *Geophys. Res. Lett*., *22*, 1877–1880, 1995.

Carslaw, K. S., T. Peter, and R. Müller, Uncertainties in reactive uptake coefficients for solid stratospheric particles, 2, Effect on ozone depletion, *Geophys. Res. Lett*., *24*, 1747–1750, 1997.

Carslaw, K. S., et al., Increased stratospheric ozone depletion due to mountain-induced atmospheric waves, *Nature*, *391*, 675–678, 1998.

Chipperfield, M. P., and J. A. Pyle, Model sensitivity studies of Arctic ozone depletion, *J. Geophys. Res*., *103*, 28,389–28,403, 1998.

Coy, L., E. R. Nash, and P. A. Newman, Meteorology of the polar vortex: Spring 1997, *Geophys. Res. Lett*., *24*, 2693–2696, 1997.

Crutzen, P. J., and F. Arnold, Nitric acid cloud formation in the cold Antarctic stratosphere: A major cause for the springtime 'ozone hole,' *Nature*, *324*, 651–655, 1986.

Curtis, A. R., and W. P. Sweetenham, Facsimile/Chekmat user's manual, 135 pp., Comput. Sci. and Syst. Div., Harwell Lab., Oxford, England, 1987.

Daniel, J. S., S. M. Schauffler, W. H. Pollock, S. Solomon, A. Weaver, L. E. Heidt, R. R. Garcia, E. L. Atlas, and J. F. Vedder, On the age of stratospheric air and inorganic chlorine and bromine release, *J. Geophys. Res*., *101*, 16,757–16,770, 1996.

DeMore, W. B., S. P. Sander, C. J. Howard, A. R. Ravishankara, D. M. Golden, C. E. Kolb, R. F. Hampson, M. J. Kurylo, and M. J. Molina, Chemical kinetics and photochemical data for use in stratospheric modeling, Evaluation number 12, *JPL Publ*., *97-4*, 1997.

Dye, J. E., D. Baumgardner, B. W. Gandrud, S. R. Kawa, K. K. Kelly, M. Loewenstein, G. V. Ferry, K. R. Chan, and B. L. Gary, Particle size distributions in arctic polar stratospheric clouds, growth and freezing of sulfuric acid droplets, and implications for cloud formation, *J. Geophys. Res*., *97*, 8015–8034, 1992.

Eskes, H. J., A. J. M. Piters, P. F. Levelt, M. A. F. Allaart, and H. M. Kelder, Variational assimilation of total-column ozone satellite data in a 2D lat-lon tracer-transport model, *J. Atmos. Sci*., in press, 2000.

Farman, J. C., B. G. Gardiner, and J. D. Shanklin, Large losses of total ozone in Antarctica reveal seasonal ClO_x/NO_x interaction, *Nature*, *315*, 207–210, 1985.

Fish, D. J., and M. R. Burton, Effect of uncertainties in kinetic and photochemical data on model predictions of stratospheric ozone depletion, *J. Geophys. Res*., *102*, 25,537–25,542, 1997.

Fortuin, J. P. F., and H. Kelder, An ozone climatology based on ozonesonde and satellite measurements, *J. Geophys. Res*., *103*, 31,709–31,734, 1998.

Ganzeveld, L. N., J. Lelieveld, and G.-J. Roelofs, A dry deposition parameterization for sulfur oxides in a chemistry and general circulation model, *J. Geophys. Res*., *103*, 5679–5694, 1998.

Hanson, D. R., and K. Mauersberger, Vapor pressures of HNO_3/H_2O solutions at low temperatures, *J. Phys. Chem*., *92*, 6167–6170, 1988.

Hanson, D. R., and A. R. Ravishankara, Reactive uptake of $ClONO_2$ onto sulfuric acid due to reaction with HCl and H_2O, *J. Phys. Chem.*, *98*, 5728–5735, 1994.

Hanson, D. R., and A. R. Ravishankara, Heterogeneous chemistry of bromine species in sulfuric acid under stratospheric conditions, *Geophys. Res. Lett.*, *22*, 385–388, 1995.

Hanson, D. R., A. R. Ravishankara, and S. Solomon, Heterogeneous reactions in sulfuric acid aerosols: A framework for model calculations, *J. Geophys. Res.*, *99*, 3615–3629, 1994.

Hanson, D. R., A. R. Ravishankara, and E. R. Lovejoy, Reaction of $BrONO_2$ with H_2O on submicron sulfuric acid aerosol and the implications for the lower stratosphere, *J. Geophys. Res.*, *101*, 9063–9069, 1996.

Harries, J. E., J. M. Russell III, A. F. Tuck, L. L. Gordley, P. Purcell, K. Stone, R. Bevilacqua, M. R. Gunson, G. Nedoluha, and W. A. Traub, Validation of measurements of water vapor from the Halogen Occultation Experiment (HALOE), *J. Geophys. Res.*, *101*, 10,205–10,216, 1996.

Hertel, O., R. Berkowicz, J. Christensen, and Ø. Hov, Test of two numerical schemes for use in atmospheric transport-chemistry models, *Atmos. Environ., Part A*, *27*(16), 2591–2611, 1993.

Houweling, S., F. D. Dentener, and J. Lelieveld, Impact of nonmethane hydrocarbon compounds on tropospheric photochemistry, *J. Geophys. Res.*, *103*, 10,673–10,696, 1998.

Huthwelker, T., T. Peter, B. P. Luo, S. L. Clegg, K. S. Carslaw, and P. Brimblecombe, Solubility of HOCl in water and aqueous H_2SO_4 to stratospheric temperatures, *J. Atmos. Chem.*, *21*, 81–95, 1995.

Jones, A. E., and J. D. Shanklin, Continued decline of total ozone over Halley, Antarctica, since 1985, *Nature*, *376*, 409–411, 1995.

Keim, E. R., et al., Measurements of the NO_y-N_2O correlation in the lower stratosphere: Latitudinal and seasonal changes and model comparisons, *J. Geophys. Res.*, *102*, 13,193–13,212, 1997.

Knudsen, B. M., Accuracy of arctic stratospheric temperature analyses and the implications for the prediction of polar stratospheric clouds, *Geophys. Res. Lett.*, *23*, 3747–3750, 1996.

Knudsen, B. M., et al., Ozone depletion in and below the Arctic vortex for 1997, *Geophys. Res. Lett.*, *25*, 627–630, 1998.

Kreher, K., G. E. Bodeker, H. Kanzawa, H. Nakane, and Y. Sasano, Ozone and temperature profiles measured above Kiruna inside, at the edge of, and outside the Arctic polar vortex in February and March 1997, *Geophys. Res. Lett.*, *26*, 715–718, 1999.

Lary, D. J., and J. A. Pyle, Diffuse radiation, twilight, and photochemistry I, *J. Atmos. Chem.*, *13*, 373–392, 1991.

Lefèvre, F., F. Figarol, K. S. Carslaw, and T. Peter, The 1997 Arctic ozone depletion quantified from three-dimensional model simulations, *Geophys. Res. Lett.*, *25*, 2425–2428, 1998.

Luo, B. P., K. S. Carslaw, T. Peter, and S. L. Clegg, Vapour pressures of H_2SO_4/HNO_3/HCl/HBr/H_2O solutions to low stratospheric temperatures, *Geophys. Res. Lett.*, *22*, 247–250, 1995.

Manney, G. L., L. Froidevaux, M. L. Santee, R. W. Zurek, and J. W. Waters, MLS observations of Arctic ozone loss in 1996–1997, *Geophys. Res. Lett.*, *24*, 2697–2700, 1997.

Müller, R., T. Peter, P. J. Crutzen, H. Oelhaf, G. P. Adrian, T. V. Clarmann, A. Wegner, U. Schmidt, and D. Lary, Chlorine chemistry and the potential for ozone depletion in the Arctic stratosphere in the winter of 1991/1992, *Geophys. Res. Lett.*, *21*, 1427–1430, 1994.

Müller, R., P. J. Crutzen, J.-U. Grooß, C. Brühl, J. M. Russell III, H. Gernandt, D. S. McKenna, and A. Tuck, Severe chemical ozone loss in the Arctic during the winter 1995–1996, *Nature*, *389*, 709–712, 1997a.

Müller, R., J.-U. Grooß, D. S. McKenna, P. J. Crutzen, C. Brühl, J. M. Russell II, and A. F. Tuck, HALOE observations of the vertical structure of chemical ozone depletion in the Arctic vortex during winter and early spring 1996–1997, *Geophys. Res. Lett.*, *24*, 2717–2720, 1997b.

Murphy, D. M., and A. R. Ravishankara, Temperature averages and rates of stratospheric reactions, *Geophys. Res. Lett.*, *21*, 2471–2474, 1994.

Newman, P. A., J. F. Gleason, R. D. McPeters, and R. S. Stolarski, Anomalously low ozone over the Arctic, *Geophys. Res. Lett.*, *24*, 2689–2692, 1997.

Nightingale, R. W., et al., Global CF_2Cl2 measurements by UARS cryogenic limb array etalon spectrometer: Validation by correlative data and a model, *J. Geophys. Res.*, *101*, 9711–9736, 1996.

Pawson, S., and B. Naujokat, Cold winters of the middle 1990s in the northern lower stratosphere, *J. Geophys. Res.*, *104*, 14,209–14,222, 1999.

Peter, T., Microphysics and heterogeneous chemistry of polar stratospheric clouds, *Annu. Rev. Phys. Chem.*, *48*, 785–822, 1997.

Portmann, R. W., S. Solomon, R. R. Garcia, L. W. Thomason, L. R. Poole, and M. P. McCormick, Role of aerosol variations in anthropogenic ozone depletion in the polar regions, *J. Geophys. Res.*, *101*, 22,991–23,006, 1996.

Prather, M. J., Numerical advection by conservation of second-order moments, *J. Geophys. Res.*, *91*, 6671–6681, 1986.

Reid, S. J., G. Vaughan, A. R. W. Marsh, and H. G. J. Smit, Accuracy of ozonesonde measurements in the troposphere, *J. Atmos. Chem.*, *25*, 215–226, 1996.

Rex, M., et al., Prolonged stratospheric ozone loss in the 1995–96 Arctic winter, *Nature*, *389*, 835–838, 1997.

Roche, A. E., et al., Validation of CH_4 and N_2O measurements by the cryogenic limb array etalon spectrometer instrument on the Upper Atmosphere Research Satellite, *J. Geophys. Res.*, *101*, 9679–9710, 1996.

Ruhnke, R., W. Kouker, T. Reddmann, H. Berg, G. Hochschild, G. Kopp, R. Krupa, and M. Kuntz, Vertical distribution of ClO at Ny-Ålesund during March 1997, *Geophys. Res. Lett.*, *26*, 839–842, 1999.

Santee, M. L., G. L. Manney, L. Froidevaux, R. W. Zurek, and J. W. Waters, MLS observations of ClO and HNO_3 in the 1996–1997 Arctic polar vortex, *Geophys. Res. Lett.*, *24*, 2713–2716, 1997.

Schulz, A., et al., Match observations in the Arctic winter 1996/1997: High stratospheric ozone loss rates correlate with low temperatures deep inside the polar vortex, *Geophys. Res. Lett.*, *27*, 205–208, 2000.

Sinnhuber, B.-M., J. Langer, U. Klein, U. Raffalski, K. Künzi, and O. Schrems, Ground-based millimeter-wave observations of Arctic ozone depletion during winter and spring of 1996/1997, *Geophys. Res. Lett.*, *25*, 3327–3330, 1998.

Solomon, S., R. R. Garcia, F. S. Rowland, and D. J. Wuebbles, On the depletion of Antarctic ozone, *Nature*, *321*, 755–758, 1986.

Steinbrecht, W., R. Neuber, P. von der Gathen, P. Wahl, T. J. McGee, M. R. Gross, U. Klein, and J. Langer, Results of the 1998 Ny-Ålesund Ozone Monitoring Intercomparison (NAOMI), *J. Geophys. Res.*, *104*, 30,515–30,523, 1999.

Strunk, M., A. Engel, M. Muller, and U. Schmidt, Estimates of total inorganic chlorine (Cl_y) using a sulfur hexafluoride derived age, in *Polar Stratospheric Ozone 1997, Proceedings of the Fourth European Symposium, 22 to 26 September, Schliersee, Bavaria, Germany*, edited by N. R. P. Harris, I. Kilbane-Dawe, and G. T. Amanatidis, pp. 393–396, Off. for Off. Publ. of the Eur. Comm., Luxembourg, 1998.

Thomason, L. W., L. R. Poole, and T. Deshler, A global climatology of stratospheric aerosol surface area density deduced from Stratospheric Aerosol and Gas Experiment II: 1984–1994, *J. Geophys. Res.*, *102*, 8967–8976, 1997.

Tiedtke, M., A comprehensive mass flux scheme for cumulus parameterization in large-scale models, *Mon. Weather Rev.*, *117*, 1779–1800, 1989.

Woodbridge, E. L., et al., Estimates of total organic and inorganic chlorine in the lower stratosphere from in situ and flask measurements during AASE II, *J. Geophys. Res.*, *100*, 3057–3064, 1995.

World Meteorological Organization (WMO), Scientific assessment of ozone depletion: 1994, *Rep. 37*, Global Ozone Res. and Monit. Proj., Geneva, 1995.

World Meteorological Organization (WMO), Scientific assessment of ozone depletion: 1998, *Rep. 43*, Global Ozone Res. and Monit. Proj., Geneva, 1999.

A. Bregman (corresponding author) and J. Lelieveld, Institute for Marine and Atmospheric Research, Princetonplein 5, 3584 CC, Utrecht, Netherlands. (bregman@phys.uu.nl)

M. M. P. van den Broek, Space Research Organization of the Netherlands, Sorbonnelaan 2, 3584 CA, Utrecht, Netherlands. (m.van.den.broek@sron.nl)

(Received September 28, 1999; revised May 9, 2000;
accepted May 11, 2000.)